On the Role of Drop Break Up for Coalescence Processes and Morphology Development in Polymer Blends under Shear

Verena E. Ziegler and Bernhard A. Wolf*

Institut für Physikalische Chemie, Johannes-Gutenberg-Universität, Jakob-Welder-Weg 13, D-55099 Mainz, Germany

Received March 9, 2005; Revised Manuscript Received April 19, 2005

ABSTRACT: Drop sizes and drop-size distributions were determined as a function of time at constant shear rates, $\dot{\gamma}$, by means of an optical shear cell in combination with an optical light microscope after preshearing the samples at high $\dot{\gamma}$. The systems under investigation were PIB 3/PDMS 152 (PIB: polyisobutylene, PDMS: poly(dimethylsiloxane), numbers: average molar masses in kg/mol) and COP 26*/PDMS 48 (COP: poly(dimethyl-*co*-methylphenylsiloxane), asterisk: apparent molar mass); all measurements refer to 25 °C. Systems and conditions were chosen such that shear rates in the vicinity of the intersection of the coalescence and the break up curves become experimentally accessible. Under these conditions, it is important to evaluate the different processes not only in terms of average drop radii but also in terms of their distribution. Such an analysis demonstrates that there exists a kind of transition from the typical behavior at low shear rates (far below the intersection, only coalescence, approach of dead-end drop radii) to that at high shear rates (far above the intersection, simultaneous coalescence and break up, approach of stationary drop radii). Within the entire transition regime between these two ordinary types of behavior, some drops are larger and others smaller than the corresponding break up radius, and the fraction of larger drops increases from zero to unity as one raises the shear rate. In some cases, one observes bimodal distributions of drop size where the ratio of the volumes of the two kinds of drops is either four or eight.

1. Introduction

How a mechanical field acts on two "immiscible" coexisting liquids depends on the particularities of the system and on the magnitude of the applied forces. In case of shear, one can distinguish four clearly separable cases in terms of shear rate $\dot{\gamma}$ and radius R of the drops of the dispersed phase. In the case of deformed drops, R stands for the radius of the equivalent sphere. For low values of $\dot{\gamma}$ and R, the dominant process will consist of coalescence, whereas break up will preferentially take place in the opposite case. If the drops are very large at low shear rates or very small at high shear rates, the converse processes will also occur. According to more detailed considerations, this situation can be described by two intersecting lines in plots of log R as a function of log $\dot{\gamma}$ (as proposed by Elmendorp[1]). One of these lines (coalescence line) states under which conditions drops do no longer merge, whereas the other (break up line) designates the limit of drop fragmentation. Only the break up line can be calculated theoretically, whereas the coalescence line is normally modeled on the basis of various simplifying assumptions.

To study coalescence processes experimentally, one usually applies high shear rates leading to small drops and reduces $\dot{\gamma}$ abruptly to the value of interest. In this manner, one can observe how the number and size of the drops change with time as a consequence of their merger. In the literature, there exist different opinions concerning the occurrence of a region in which coalescence as well as break up processes are absent. Because this region is located in the vicinity of the intersection of the two corresponding lines, we are paying special attention to it. To be able to get experimental access to that range, we have selected two chemically different systems with diverse interfacial tensions and melt viscosities of the components.

* Author to whom correspondence should be addressed. E-mail: Bernhard.Wolf@uni-mainz.de.

2. Theoretical Background

The variables determining number and shape of liquid drops suspended in another liquid during shear are: interfacial tension σ, matrix viscosity η_m, viscosity of the drop η_d, overall composition of the mixture and shear rate $\dot{\gamma}$, if one refrains at this point from the discussion of kinetic effects. The capillary number Ca quantifies the ratio between the viscous force, which tends to deform and to break the drop, and the counteracting interfacial force, which tries to minimize the surface of the drop. The capillary number is defined as

$$Ca = \frac{\dot{\gamma}\eta_m R_0}{\sigma} \tag{1}$$

where R_o is the radius of the drop in a quiescent state.

Break Up. As the capillary number surpasses a critical value, Ca_{crit}, the viscous force exceeds the interfacial force and the drop becomes unstable against break up. According to Taylor[2,3] Ca_{crit} is given by

$$Ca_{crit} = 0.5\frac{16\lambda + 16}{19\lambda + 16} \tag{2}$$

where

$$\lambda = \frac{\eta_d}{\eta_m} \tag{3}$$

10.1021/ma050504n CCC: $30.25
Published on Web 05/21/2005

DeBruijn[4] has fitted experimental data of Grace[5] and of his own and obtained the following equation for Ca_{crit}

$$\log Ca_{crit} = -0.506 - 0.0994 \log \lambda + 0.124(\log \lambda)^2 - \frac{0.115}{\log \lambda - \log 4.08} \quad (4)$$

If a reliable value for Ca_{crit} is accessible in terms of viscosity ratios λ (eqs 3 and 4) and σ is known, the radius of the drops that are just stable against break up at a given shear rate can be easily forecast by means of eqs 4 and 1. This characteristic radius is in the following called $R^{DeBruijn}$.

Coalescence. The process of shear-induced coalescence can be described by the eqs (5−7) of Janssen and Meijer[6] and Janssen[7] following the models of Chester.[8,9] To coalesce, two drops first have to meet and, second, stay together long enough to allow the separating matrix film to drain; for sufficiently long measuring times, the collision probability can be set at 1. The collision time is inversely proportional to the shear rate; during this period, the matrix film has to reach a critical thickness h_{crit} at which it becomes unstable because of van der Waals forces and disrupts. If the collision time is too short or if the drops are too big, the amount of the matrix film that has to be removed becomes too large and the film thickness will not reach its critical value, i.e., the two drops come apart without any change. Three models for the maximum size the drop can reach via coalescence are distinguished regarding the mobility of the interface: immobile interface (IMI), partially mobile interface (PMI), and fully mobile interface (FMI):

$$\text{IMI:} \quad R = \left(\frac{8}{9}\right)^{1/4} h_{crit}^{1/2} \left(\frac{\eta_m \dot{\gamma}}{\sigma_{12}}\right)^{-1/2} \quad (5)$$

$$\text{PMI:} \quad R = \left(\frac{16}{3}\right)^{1/5} \left(\frac{h_{crit}}{\lambda}\right)^{2/5} \left(\frac{\eta_m \dot{\gamma}}{\sigma_{12}}\right)^{-3/5} \quad (6)$$

$$\text{FMI:} \quad R \ln\left(\frac{R}{h_{crit}}\right) = \left(\frac{2}{3}\right) \left(\frac{\eta_m \dot{\gamma}}{\sigma_{12}}\right)^{-1} \quad (7)$$

For binary polymer blends, the PMI model gives the best accordance with the experimental data in the most cases,[10−13] but the IMI model can also be suited.[14,15] The critical film thickness and, therefore, the drop size should be independent of concentration, but this does not necessarily hold true, as shown by results of Sundararaj and Macosko,[16] Minale et al.,[10] and Vinckier et al.[17]

Elmendorp Diagram. For the discussion of the fundamental features of the shear-rate dependence of the radii of the smallest drops formed by break up (R^{br}) and of the largest drops resulting from coalescence (R^{coal}), we use the representation suggested by Elmendorp.[1]

According to Figure 1, one can distinguish four different areas in the $R-\dot{\gamma}$ plane, which are defined by the break up and coalescence lines. Within region I, the drops become smaller, and within region II, they become larger by shear. Region III represents a zone where they are too small to be broken and too large to coalesce. Finally, inside region IV, both processes can take place simultaneously. For constant temperature, the positions of the two characteristic lines of the Elemendorp diagram depend on the particular system and on the mixing ratio of the components; this means that the location of their intercept point (at $\dot{\gamma}^*$ and R^*) may vary widely.

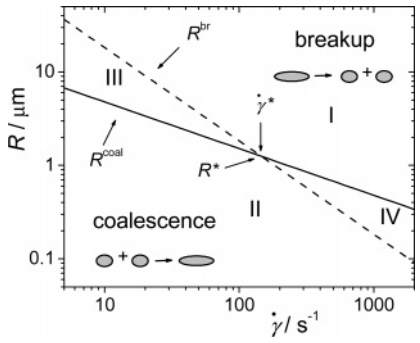

Figure 1. Schematic (Elmendorp) diagram displaying the limiting radii of drops suspended in another liquid achieved under stationary shear by coalescence or break up.

Table 1. Molar Masses (As Obtained from GPC Measurements) and Viscosities of the Polymers

polymer	M_n/kg mol^{-1}	M_w/kg mol^{-1}	$\eta^{25\ °C}$/Pa s
PDMS152	80.9	152.1	69.7
PIB3	1.3	2.6	26.9
PDMS48	29.5	48.5	2.2
COP26*	5.2*	26.4*	1.2

3. Experimental Section

Polyisobutylene (PIB 3) was kindly donated by BASF, Germany, the two poly(dimethylsiloxane)s (PDMS 152 and PDMS 48) by Wacker, Germany. The poly(dimethyl-*co*-methylphenylsiloxane) (COP 26*) was purchased from Roth, Germany. The numbers after the abbreviation state the weight-average molar masses in kg/mol. These data were obtained by means of GPC measurements in THF (PIB) or toluene (PDMS and COP 26*) using polystyrene standards and applying universal calibration. Because the Kuhn−Mark−Houwink parameters were not known for COP 26*, we used the corresponding data for PDMS to obtain an apparent molar mass indicated by an asterisk. According to ^{1}H NMR measurements, this polymer contains 30% methylphenyl units. At room temperature, COP 26* is practically immiscible with PDMS 48. Viscosities were measured with the shear-controlled rheometer CV 100 from Haake, Germany and with the stress-controlled rheometer AR 1000 from TA instruments, USA. Within the investigated range of shear rates (0−50 s^{-1} for PIB 3/PDMS 152 and 0−100 s^{-1} for COP 26*/PDMS 48), all polymers behave Newtonian. The characteristic data of the polymers are collected in Table 1.

The interfacial tensions σ at 25 °C were determined by the method of drop retraction as described by Guido and Villone[18] using the optical shear cell CSS 450 from Linkam Scientific, UK. Further details can be found in the literature.[19] For PIB 3 drops in PDMS 152, we obtained $\sigma = 1.78$ mNm^{-1}. This value differs considerably from that resulting for the opposite case (PDMS 152 in PIB 3) where $\sigma = 2.25$ mNm^{-1}. The reason for this pronounced influence of the overall composition of the system on the measured interfacial tension lies in the broad molecular-weight distribution of the components as discussed extensively earlier.[19,20] For the system COP 26*/PDMS 48, the difference of σ resulting from the exchange of matrix and drop phase remains small, PDMS 48 in COP 26* yields $\sigma = 0.44$ mNm^{-1} as compared with $\sigma = 0.49$ mNm^{-1} for COP 26* in PDMS 48.[19]

The morphology development during shear was observed with the optical shear cell CSS 450. The gap was kept between 50 μm for high shear rates up to 250 μm for the low shear rates. In most cases, the gap was at least 10 times the final drop radius R; for some experiments we had to set it at 6 times R. The samples were prepared by stirring the blends with a spatula by hand for 3 min. After that, vacuum was applied

until all air bubbles were removed; the time required for that purpose ranged from 5 min up to 4 h. Thereafter, the sample was placed into the shear cell and was presheared for 5 min at 100 or 50 s^{-1}. This procedure suffices to eradicate the sample history. After that treatment, $\dot{\gamma}$ was rapidly reduced to a preselected value, and the morphology development was observed by taking digital images of the sheared sample at different times.

To determine the zero-shear radii, R_o, the micrographs were analyzed with the help of the software Optimas 6.1, Mediacybernetics, USA, by extracting manually the main axis L_{app} of at least 200 drops. With the CSS 450 instrument, the direction of observation is perpendicular to the plane of shear. Because the main axis of a deformed drop is normally not aligned in the plane of shear, it is with this setup only possible to see the projection of the main axis. For that reason, we have established a correlation function between L_{app} and R_0 in the following manner. The blend was sheared at a certain shear rate until the drops took their equilibrium shape. Then, shear was stopped and images were taken very rapidly during the relaxation period. From the last image of the sheared drop and an image taken after its complete relaxation, the elongated axis and the diameter in quiescent state were evaluated for about 50 drops. In this manner, one obtains a correlation between these two parameters for the different shear rates, which enables the calculation of R_0 from the observed L_{app}.

We used two different averages of drop size to quantify polydispersity: the number average R_N, and the volume average R_V; furthermore, we determined the mean value of the Gaussian fit to the drop size distribution R_G. The following relations hold true

$$R_N = \frac{\sum_{i=1}^{\infty} n_i R_i}{\sum_{i=1}^{\infty} n_i} \tag{8}$$

$$R_V = \frac{\sum_{i=1}^{\infty} n_i R_i^4}{\sum_{i=1}^{\infty} n_i R_i^3} \tag{9}$$

$$y = y_0 + \frac{A}{SD\sqrt{2\pi}} \exp^{-(R-R_G)^2/2SD^2} \tag{10}$$

SD: standard deviation

4. Results and Discussion

The viscosity ratio of all blends investigated here is below unity ($\lambda = 0.552$ for COP 26*/PMDS 48 and 0.386 for PIB 3/PDMS 152). The following report is divided into three parts: the first shows the time development of the size of the suspended drops resulting from coalescence after a step down in shear rate, the second part discusses the results in terms of an Elmendorp diagram, and the third part deals with break up processes taking place in the course of coalescence.

4.1. Coalescence. Shortly after a step down in shear rate, the drop-size distribution can be fitted by a Gaussian function. As time proceeds, a small number of very large drops are formed via coalescence, which means that the distribution develops a tail at high R values and is no longer Gaussian. This is, together with a micrograph of the sheared sample, demonstrated in Figure 2 for 15 vol % COP 26* in PDMS 48 at 5 s^{-1} and in Figure 3 for 5 vol % PIB 3 in PDMS 152 at 2 s^{-1}. These two examples belong to a special group of experiments for which the tailing is so pronounced that the drop size distribution develops a second peak that can be analyzed separately. This behavior also arises for $\varphi_{PDMS\ 48} = 0.949$ at $\dot{\gamma} = 5$ and 10 s^{-1} and for $\varphi_{PDMS\ 152} = 0.950$ at $\dot{\gamma} = 1$ s^{-1}. Although it is in some cases unrealistic to fit the drop size distributions according to Gauss, these curves are also shown in Figure 2 and in Figure 3 to visualize the asymmetry of the distributions.

The mean drop radii R_V and R_N are shown in the next figures for $\varphi_{PDMS\ 48} = 0.949$ (Figure 4 a), $\varphi_{PDMS\ 48} = 0.850$ (Figure 4b), and $\varphi_{PDMS\ 152} = 0.950$ (Figure 5) as a function of strain $\gamma = \dot{\gamma}t$. Because of the logarithmic scale of the ordinate, one can in these graphs immediately read the polydispersity (R_V/R_N) of the drops. For the present blend ($\lambda < 1$), the polydispersities are higher than for the inverse blend ($\lambda > 1$)[21] but they remain below two. Values larger than two have been reported for chemically different systems.[22,23]

It would be interesting to find some general laws to calculate or at least to estimate the strain required to achieve constant drop size under the different experimental conditions. However, the present results do not reveal a clear-cut trend. For 15 vol % COP 26* in PDMS 48, it takes about 350 000 strain units at $\dot{\gamma} = 10$ s^{-1}; for 5 vol % PIB 3 in PDMS 152 and the same shear rate, it is reached within one minute (600 strain units). Most cases require about 200 000−300 000 strain units to reach constant drop size. Diverse values are also reported by other authors: 100 up to 100 000 by Ramic et al.,[23] 15 000−20 000 by Minale et al.[11] and at least 165 000 by Rusu and Peuvrel-Disdier.[12]

Another interesting feature concerns the drop growth rate immediately after the step down in shear rate. A preliminary evaluation of the present data reveals that R increases with time t more than exponentially. Plots of log R vs log t look similar to the theoretical curves presented by Rother and Davis.[24]

4.2. Elmendorp Diagrams. The Elmendorp diagrams of the three investigated mixtures are shown in Figures 6−8. They represent three different cases: For $\varphi_{PDMS\ 48} = 0.949$, the final average coalescence radii are in all cases located left of the intersection of the lines in the Elmendorp diagram (Figure 6). In this case, the IMI model describes the coalescence radii best. With the next blend ($\varphi_{PDMS\ 48} = 0.850$), the corresponding data cover the region of intersection (Figure 7); these results are better reproduced by the PMI model. For the third case ($\varphi_{PDMS\ 152} = 0.950$), all time independent radii fall on the right-hand side of the intersection (Figure 8); the PMI model is again better suited than the IMI model. This assessment should not, however, be overinterpreted not only because of the limited number of experimental points of Figure 7 and Figure 8, but also because of other reasons discussed later. According to literature,[10,1,11] the experiments shown in the last three diagrams should correspond to coalescence only (Figure 6) and to coalescence and break up (Figure 8). With one system, one can observe the transition between these features (Figure 7).

4.3. Co-occurrence of Coalescence and Break Up. In various experiments, one could see shear-induced drop rupture in the microscope. Figure 9 shows an example for this observation. These pictures give the impression of a bimodal drop distribution. That this is indeed the case, as can be seen from Figure 3, referring to these experiments.

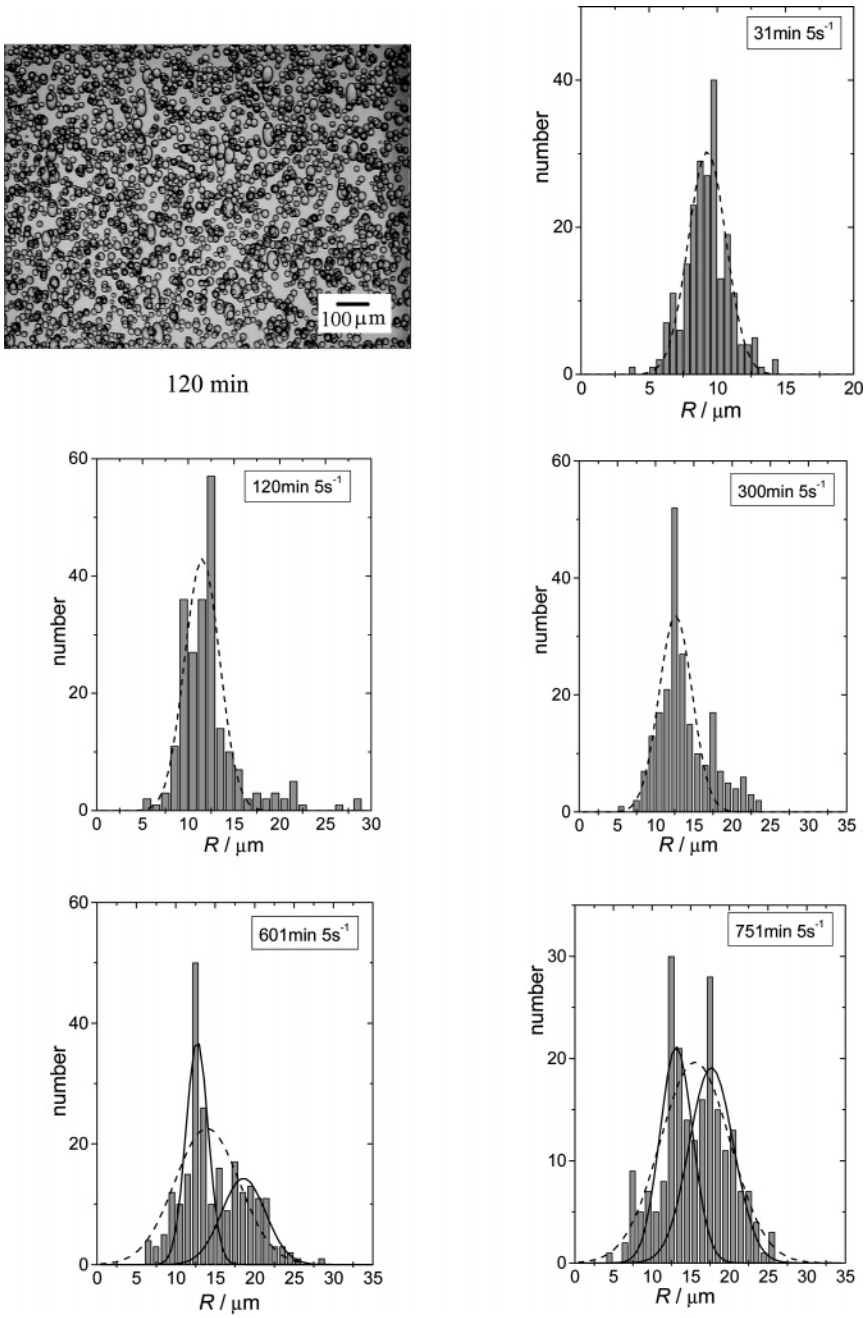

Figure 2. Drop size distribution for COP 26*/PDMS 48 and $\varphi_{PDMS\ 48} = 0.850$ at different times after decreasing the shear rate from 100 to 5 s^{-1}. The broken curves are Gaussian fits to the entire distributions. For long times, where the bimodality becomes definite, the two parts are evaluated separately (full lines).

All (Figure 6) or most (Figure 7) of the *average* final drop radii are located below the corresponding break up radii. One is therefore tempted to conclude that no break up can take place once the final dimensions are reached. However, upon a more detailed evaluation one can see drops, which are considerably larger than calculated according to the equation of DeBruijn (4) for the maximum size of stable drops. Such observation were made with $\varphi_{PDMS\ 48} = 0.949$ at $\dot{\gamma} = 5$, 10, and 20 s^{-1} and with $\varphi_{PDMS\ 48} = 0.850$ at 2 s^{-1}.

To analyze this situation quantitatively, we subdivide the drop distribution into two parts at $R^{DeBruijn}$. In this manner, we obtain the corresponding average radii, $R^{<Rb}$, for the population below this divide and, $R^{>Rb}$, the population above it (whenever we can see a sufficiently large number of drops for both populations). Figure 10 and Figure 11 show examples for the results concerning the evolution of the average drop dimensions of the two populations and that of the fraction Φ of all drops with $R^{>Rb}$ (number of drops with $R^{>Rb}$ divided by the total drop number). The most surprising feature of this analysis consists of the fact that $R^{>Rb}$ and $R^{<Rb}$ become constant considerably faster than Φ.

In all experiments in which we could observe a sufficiently large number of drops with $R^{>Rb}$ and $R^{<Rb}$, these two types of drops reach constant average radii after relatively short times. If the drops are very small after preshear, i.e., far below $R^{DeBruijn}$, and if their concentration is low, it takes more time until the first drops with $R^{>Rb}$ appear than with larger drops and higher drop concentrations. In all cases, Φ grows as time proceeds and reaches a constant value that depends on shear rate and composition. Decreasing the volume fraction of PDMS from $\varphi_{PDMS\ 48} = 0.949$ to 0.850

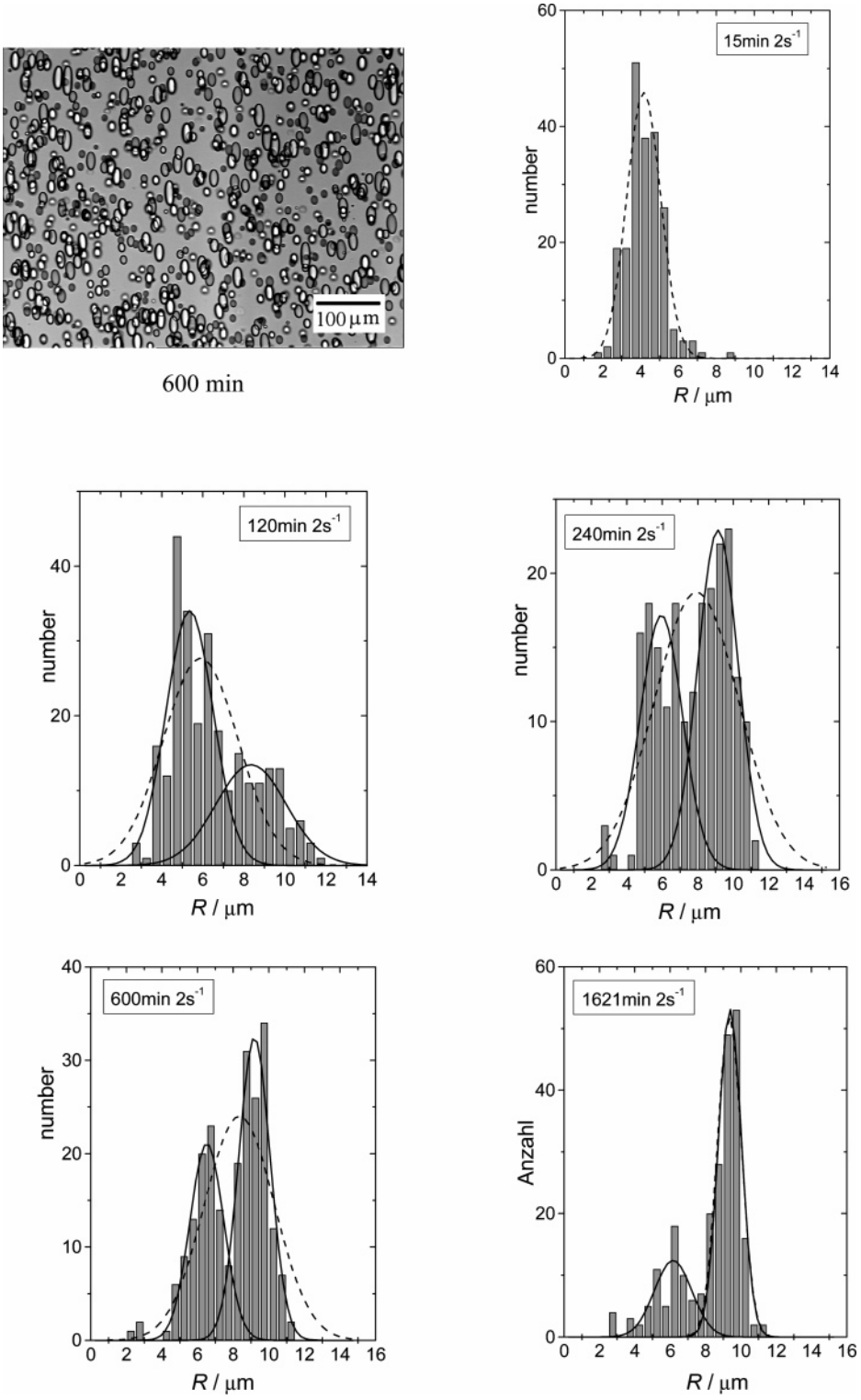

Figure 3. Drop size distributions for PIB 3/PDMS 152 and $\varphi_{\mathrm{PDMS\ 152}} = 0.950$ at different times after decreasing the shear rate from 50 to 2 s^{-1}. The broken curves are Gaussian fits to the entire distributions. For longer times, where bimodality becomes definite the two parts are evaluated separately (full lines).

increases Φ from $\cong 0$ to 0.110 for $\dot{\gamma} = 5\ s^{-1}$; for $\dot{\gamma}$ values of 10 and 20 s^{-1}, these data read 0.060 to 0.663 and 0.043 to 0.967, respectively. A similar augmentation of the above ratio is caused by an increase in shear rate: for $\varphi_{\mathrm{PDMS\ 48}} = 0.850$ from 0.110 at $\dot{\gamma} = 5\ s^{-1}$ via 0.663 at 10 s^{-1} to 0.967 at 20 s^{-1}. The above statement concerning the influence of $\dot{\gamma}$ remains true for the other system under investigation. For $\varphi_{\mathrm{PDMS\ 152}} = 0.950$ and $\dot{\gamma} = 1\ s^{-1}$, $\Phi = 0.58$; it rises to 0.874 for 2 s^{-1} and reaches unity at 5 s^{-1}. In the latter case, the average size of the drops with $R^{<\mathrm{Rb}}$ becomes constant within a short time, and the number of these drops decreases so rapidly that it becomes practically zero before the drops with $R^{>\mathrm{Rb}}$ reach their constant value. From this time on $\Phi = 1$.

In view of the central importance of the intersection (parameters marked by an asterisk) of the two characteristic lines in Elemendorp diagrams for the observed phenomena and to be able to compare the behavior of

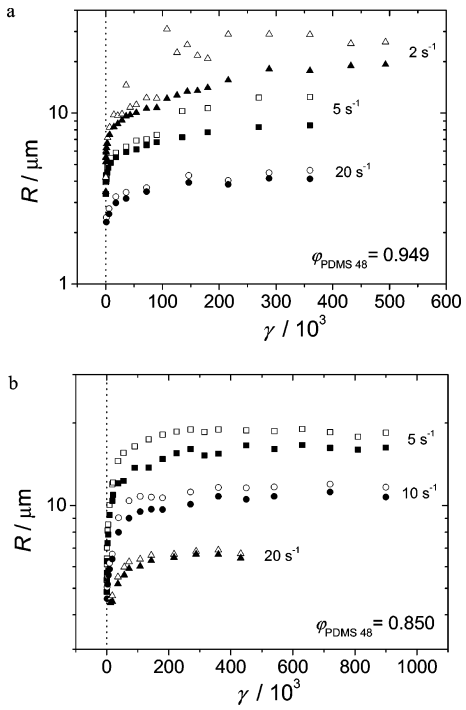

Figure 4. R_V (open symbols) and R_N (full symbols) for COP 26*/PDMS 48 and $\varphi_{PDMS\ 48} = 0.949$ (a) or $\varphi_{PDMS\ 48} = 0.850$ (b) as a function of strain, after reducing the shear rate from 100 s^{-1} to the indicated values.

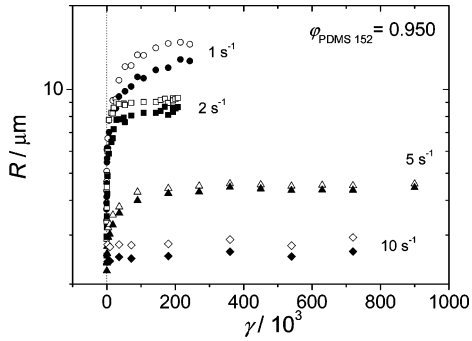

Figure 5. R_V (open symbols) and R_N (full symbols) for PIB 3/PDMS 152 and $\varphi_{PDMS\ 152} = 0.950$ as a function of strain, after reducing the shear rate from 50 s^{-1} to the indicated values.

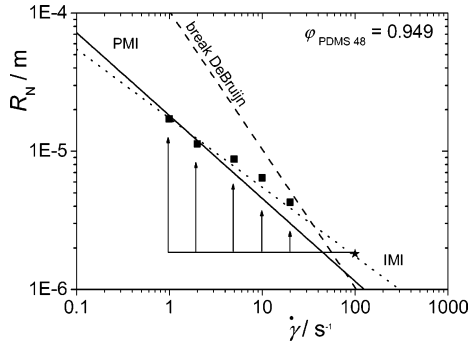

Figure 6. Time-independent R_N values as a function of shear rate for COP 26*/PDMS 48 and $\varphi_{PDMS\ 48} = 0.949$. Arrows indicate the experimental paths; full star: drop size after preshearing at 100 s^{-1}. Dashed line: break up DeBruijn; dotted line: coalescence IMI model, $h_c = 1.411$ μm; solid line: coalescence PMI model, $h_c = 0.098$ μm.

different systems, we introduce reduced axes as $\tilde{R}_N = R_N/R_N^*$ and $\tilde{\dot{\gamma}} = \dot{\gamma}/\dot{\gamma}^*$. Figure 12 shows the average time-independent drop sizes together with $R^{>Rb}$ and $R^{<Rb}$.

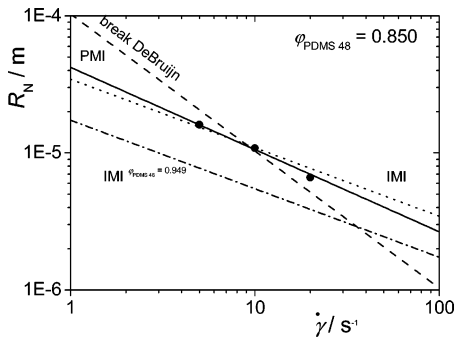

Figure 7. Time-independent R_N as a function of shear rate for COP 26*/PDMS 48 with $\varphi_{PDMS\ 48} = 0.850$ after a step down of shear rate from 100 s^{-1}; dashed line: break up curve according to DeBruijn plus coalescence curves according to the IMI model (dotted line, $h_c = 5.588$ μm) and the PMI model (solid line, $h_c = 0.811$ μm). The fourth line (dot−dash) is the coalescence curve for $\varphi_{PDMS\ 48} = 0.949$ from Figure 6. Immediately after the step down in shear rate, the optical density of the sample is too high to allow the determination of drop radii. According to results shown in Figure 6, the drop radius immediately after preshear at 100 s^{-1} is ≥ 1.8 μm.

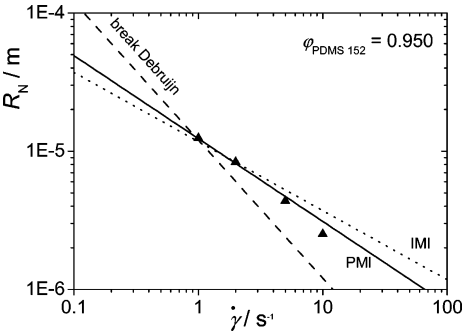

Figure 8. Time-independent R_N values as a function of shear rate for PIB 3/PDMS 152 with $\varphi_{PDMS\ 152} = 0.950$; dashed line: break up curve according to DeBruijn plus coalescence curves according to the IMI model (dotted line, $h_c = 5.662$ μm) and the PMI model (solid line, $h_c = 0.682$ μm). Immediately after the step down in shear rate, the optical density of the sample is too high to allow the determination of drop radii. According to experiments for $\varphi_{PDMS\ 152} = 0.990$, the drop radius immediately after preshear at 50 s^{-1} is ≥ 1.5 μm.

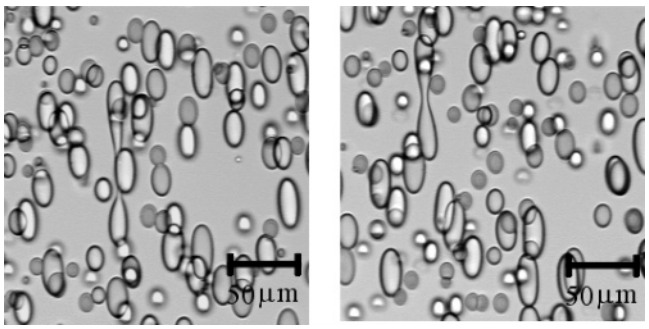

Figure 9. Two micrographs documenting drop break up during coalescence, 1200 min after the shear step, for PIB 3/PDMS 152 with $\varphi_{PMDS\ 152} = 0.950$ at $\dot{\gamma} = 2$ s^{-1}.

The data in the vicinity of the intersection superimpose so that not all can be seen.

The results shown in Figure 12 indicate that steady-state drop sizes via coalescence and break up can be reached not only in region IV of the Elmendorp diagram (Figure 1) but also in region III not too far from the intersection of the coalescence and break up lines. The average drop size is then dominated by the particular

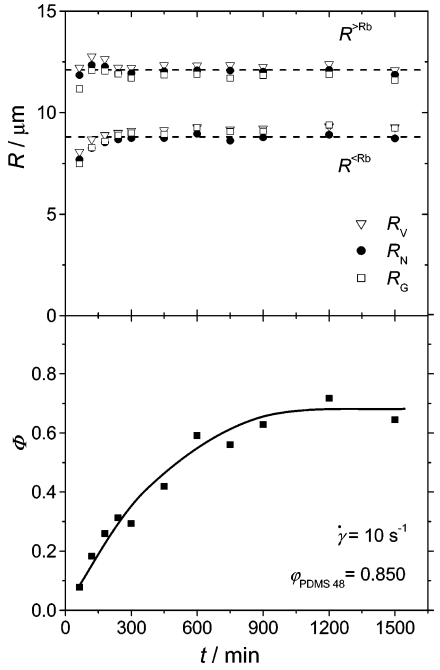

Figure 10. $R_N, R_V, R_G > R^{DeBruijn}$, and $< R^{DeBruijn}$ (upper part) and Φ (lower part) as a function of time for COP 26*/PDMS 48 with $\varphi_{PMDS\ 48} = 0.850$ at $\dot{\gamma} = 10\ s^{-1}$. The dashed lines are the time-independent values of the R_N, the solid curve is drawn as a guide for the eye.

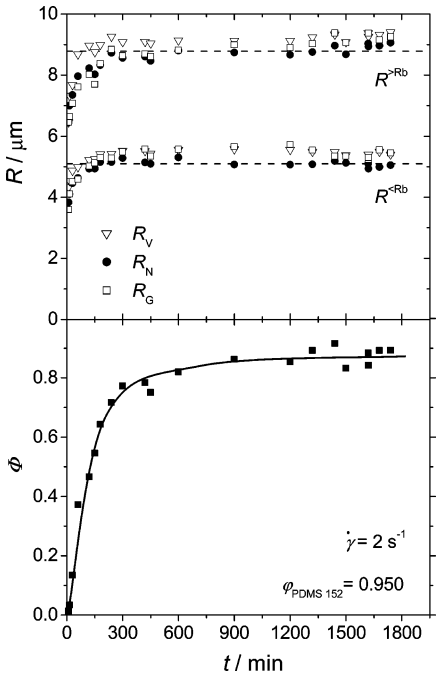

Figure 11. $R_N, R_V, R_G > R^{DeBruijn}$, and $< R^{DeBruijn}$ (upper part) and Φ as function of time for PIB 3/PDMS 152 where $\varphi_{PMDS\ 152} = 0.950$ $\dot{\gamma} = 2\ s^{-1}$. The dashed lines are the average values of R_N for $t >$ 300 min; the solid line is drawn as a guide for the eye.

value of Φ. For $\tilde{\dot{\gamma}} \ll \tilde{\dot{\gamma}}*$, Φ approaches zero, and for $\tilde{\dot{\gamma}} \gg \tilde{\dot{\gamma}}*$, it tends to unity.

As can be seen in Figure 2 and in Figure 3, some drop-size distributions become bimodal during the final stage of the experiments. Once bimodality is established, the average radii for the two peaks (evaluated separately) are time independent as shown in Figure 13 and Figure 14 for two examples.

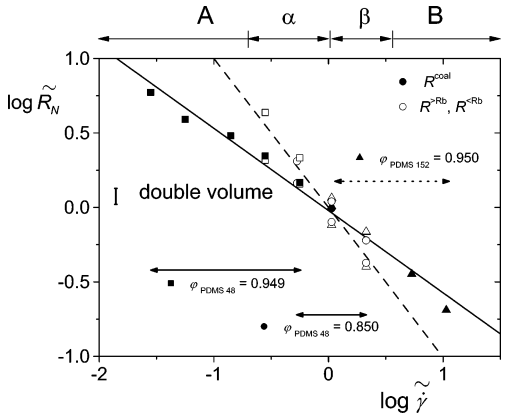

Figure 12. Full symbols: reduced number-average radii; open symbols: reduced number-average radii *by analyzing the drop size distribution according to* $R > R^{DeBruijn}$ *and* $< R^{DeBruijn}$. The reduction parameters are the intersection points of the coalescence curve and the curve. The arrows shown above the graph indicate the ranges of reduced shear rate discussed in the conclusion.

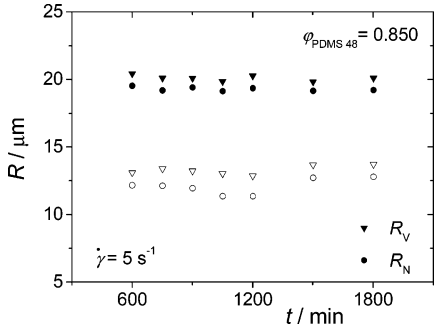

Figure 13. R_N and R_V resulting from the separate analysis of the two peaks of the drop size distribution as function of time for COP 26*/PDMS 48 and $\varphi_{PMDS\ 48} = 0.850$ at $\dot{\gamma} = 5\ s^{-1}$.

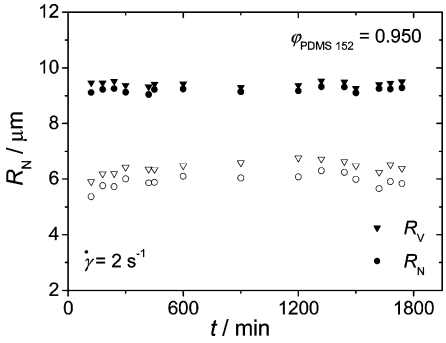

Figure 14. R_N and R_V resulting from the separate analysis of the two peaks of the drop size distribution as function of time for PIB 3/PDMS 152 and $\varphi_{PMDS\ 152} = 0.950$ at $\dot{\gamma} = 2\ s^{-1}$.

To be able to compare the results concerning bimodal drop distribution obtained with the different blends, they are also plotted conjointly in the normalized Elmendorp diagram shown in Figure 15.

If one assumes that coalescence is favored between two drops with the same radii as is recommended by Wang et al.[22,25] and that break up preferentially yields two drops of equal size, we can calculate drops of what size should be formed upon the rupture of the large drops and upon the coalescence of the small drops. It is interesting to note that the volume of big drops is in four cases four times larger than that of the small drops. A formal interpretation would imply that two intermediate drop populations (not seen in microscope) are involved in the dead-end case as well as under station-

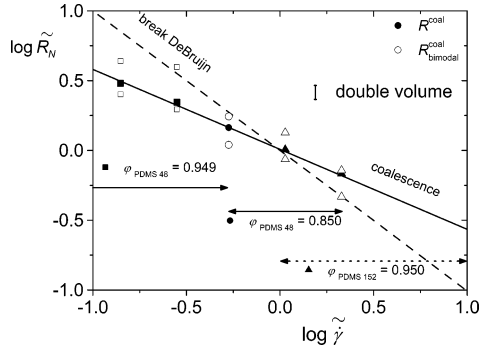

Figure 15. Full symbols: reduced number-average radii; open symbols: reduced number-average radii *by analyzing the two peaks of the bimodal size distribution*. The reduction parameters are the intersection points of the coalescence curve and the curve. The bar indicates the change in drop radii upon doubling or halving their volume.

ary-state conditions. In one case (left-most point in Figure 15), it needs three intermediate drop sizes (factor eight in the drop volumes of the two populations). The above considerations are only valid for R_N.

5. Conclusion

A common validation of the different experiments presented in the previous section demonstrates that the coalescence processes are only proceeding as expected from literature and from theoretical considerations as long as the shear rates are sufficiently different from the value fixed by the intersection of the coalescence and break up lines in the Elemendorp diagram. On the basis of the present findings, we discriminate these different regions of shear rate by means of the measured drop-size distributions. If its width is at a given shear rate less than the distance between the coalescence and break up line, one observes normal behavior, i.e., the coalescence comes to a dead at end for $\dot{\gamma} \ll \dot{\gamma}^*$ ($\dot{\gamma}^*$: intersection of coalescence and break up lines) and a stationary state is reached for all drops at $\dot{\gamma} \gg \dot{\gamma}^*$. To facilitate the discussion, we call these ranges of shear rates (cf. Figure 12) A on the low $\dot{\gamma}$ side and B on the high $\dot{\gamma}$ side. On the other hand, if the width of the distribution becomes equal to or larger than the distance between the coalescence and the break up line, extra phenomena emerge. Again, we distinguish between a range α straight left of $\dot{\gamma}^*$ and β straight right of it.

The most outstanding observation consists of the existence of drops with radii larger than the break up radius in region α. The drop-size distribution may be unimodal or bimodal within the regions α and β, where we could so far not find a criterion why we observe one case or the other. Time-independent average drop sizes are reached in all cases. Upon subdividing both types of distributions into two parts at the calculated break up radius, one obtains two characteristic additional average values, one for the smaller and one for the larger drops. The time-independent number fraction, Φ_∞, of drops of the larger kind ($R^{>Rb}$) varies systematically with shear rate in the vicinity of the $\dot{\gamma}^*$. $\Phi_\infty = 0$ at the border between A and α. As one increases the shear rate, Φ_∞ rises and approaches $\Phi_\infty = 1$ at the border between range β and B. One may speculate that Φ_∞ becomes 0.5 at the intersection between the coalescence and the break up line. In this context, it is worthwhile to note that the average drop sizes of the smaller part and of the larger part of the distribution become constant much earlier as the coalescence processes proceed than Φ, the number fraction of larger drops.

Another interesting feature could be observed by means of a modified analysis of the bimodal distributions. Splitting them in their minimum (instead of the break up radius) into two portions, one can calculate number-average volumes for the smaller and for the larger drops. Assuming that drops normally double their volume upon coalescence and half it upon break up, it is possible to estimate how many such events should lie between the peaks of bimodality. For four experiments, it turned out that two steps are required; in one experiment, it needs one step more. In no case was it possible to see the "intermediate" drops postulated by these considerations. One may speculate that their lifetime is too short to offer a reasonable chance of direct observation. Another explanation could be that the drops of at least one population reach dead-end dimensions.

Acknowledgment. We would like to thank the "Arbeitsgemeinschaft Industrieller Forschungsvereinigungen", which finances this research (project numbers 12216N and 13792N).

References and Notes

(1) Elmendorp, J. J.; Van der Vegt, A. K. *Polym. Eng. Sci.* **1986**, *26*, 1332−1338.
(2) Taylor, G. I. *Proc. R. Soc. London, Ser. A* **1934**, *146*, 501−523.
(3) Taylor, G. I. *Proc. R. Soc. London, Ser. A* **1932**, *138*, 41−48.
(4) DeBruijn, R. A. Dissertation, University of Technology, Eindhoven, 1989.
(5) Grace, H. P. *Chem. Eng. Commun.* **1982**, *14*, 225−277.
(6) Janssen, J. M. H.; Meijer, H. E. H. *Polym. Eng. Sci.* **1995**, *35*, 1766−1778.
(7) Janssen, J. M. H. Dissertation, University of Technology, Eindhoven, 1993.
(8) Chesters, A. K. In *International Conference on Turbulent Two-Phase Flow Systems, Toulouse, France*, 1988; p 234.
(9) Chesters, A. K. *Int. J. Multiphase Flow* **1975**, *2*, 191.
(10) Minale, M.; Mewis, J.; Moldenaers, P. *AIChE J.* **1998**, *44*, 943−950.
(11) Minale, M.; Moldenaers, P.; Mewis, J. *Macromolecules* **1997**, *30*, 5470−5475.
(12) Rusu, D.; Peuvrel-Disdier, E. *J. Rheol.* **1999**, *43*, 1391−1409.
(13) Grizzuti, N.; Bifulco, O. *Rheol. Acta* **1997**, *36*, 406−415.
(14) Tucker, C. L.; Moldenaers, P. *Annu. Rev. Fluid Mech.* **2002**, *34*, 177−210.
(15) Jansseune, T.; Mewis, J.; Moldenaers, P.; Minale, M.; Maffettone, P. L. *J. Non-Newtonian Fluid Mech.* **2000**, *93*, 153−165.
(16) Sundararaj, U.; Macosko, C. W. *Macromolecules* **1995**, *28*, 2647−2657.
(17) Vinckier, I.; Moldenaers, P.; Terracciano, A. M.; Grizzuti, N. *AIChE J.* **1998**, *44*, 951−958.
(18) Guido, S.; Villone, M. *J. Colloid Interface Sci.* **1999**, *209*, 247−250.
(19) Ziegler, V. E.; Wolf, B. A. *Langmuir* **2004**, *20*, 8688−8692.
(20) Shi, T.; Ziegler, V. E.; Welge, I. C.; An, L.; Wolf, B. A. *Macromolecules* **2004**, *37*, 1591−1599.
(21) Ziegler, V. E.; Wolf, B. A. *arXive*, **2005**, *cond-mat/0504479*, 20 Apr 2005.
(22) Lyu, S. P.; Bates, F. S.; Macosko, C. W. *AIChE J.* **2000**, *46*, 229−238.
(23) Ramic, A. J.; Hudson, S. D.; Jamieson, A. M.; Manas Zloczower, I. *Polymer* **2000**, *41*, 6263−6270.
(24) Rother, M. A.; Davis, R. H. *AIChE J.* **2003**, *49*, 546−548.
(25) Wang, H.; Zinchenko, A. Z.; Davis, R. H. *J. Fluid Mech.* **1994**, *265*, 161.

MA050504N